OPTIMAL CONTROL OF AN UNDERSEA GLIDER IN A SYMMETRIC PULL-UP

R. Kraus, E. Cliff, C. Woolsey, and J. Luby

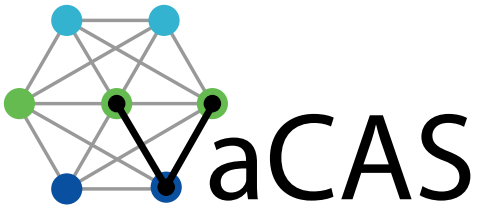

Virginia Center for Autonomous Systems
Virginia Polytechnic Institute & State University
Blacksburg, VA 24060
www.unmanned.vt.edu

October 24, 2008

Technical Report No. VaCAS-2008-03

The views expressed in this article are those of the author and do not reflect the official policy or position of the United States Air Force, Department of Defense, or the U.S. Government.

Summary

An undersea glider is a winged autonomous undersea vehicle which modulates its buoyancy to rise or sink and moves its center of mass to control pitch and roll attitude. By properly phasing buoyancy and pitch control, an undersea glider rectifies the vertical motion caused by changes in buoyancy into forward motion caused by the lift force on the fixed wing. The characteristic "porpoising" motion is useful in oceanographic surveys and the propulsion method is extremely efficient – undersea gliders routinely operate for months without human intervention. Glider efficiency could be improved even further by addressing the phenomenon of "stall" (loss of lift) when a glider transitions from downward to upward flight. Because the stall phenomenon occurs asymmetrically over the vehicle's wing, it can cause directional errors which must be corrected at a corresponding energetic cost. This paper describes the formulation of a point mass model and its dynamic equations of motion. An optimal control formulation was designed using angle of attack and buoyancy as controls to investigate control scheduling methods for avoiding stall in a symmetric pull-up. The calculations were repeated using three different numerical solution techniques for comparison of the methodologies and results. The model was updated to include longitudinal rigid body dynamics and changed the control to the rate of change of the longitudinal center of gravity location. This model allowed for the inclusion of added mass effects due to fluid displacement.

Contents

List of Figures

List of Tables

1 Introduction

Buoyancy-driven undersea gliders are highly efficient winged underwater vehicles which locomote by modifying their internal shape. In the typical actuation scheme, a servo-actuator shifts the center of mass relative to the center of buoyancy and a buoyancy bladder modulates the glider's net weight (weight minus buoyancy). By appropriately cycling these actuators, the vehicle can control its directional motion and propel itself with great efficiency. Examples of undersea gliders include *Slocum* [13], *Seaglider* [3], and *Spray* [12].

Undersea gliders locomote by repeatedly descending and ascending in a sawtooth pattern. The locomotive efficiency owes to the fact that these vehicles spend much of their time in steady, gliding flight. Little control effort is required except at transition points, where the glider switches from downward to upward flight or vice versa. Early efforts to design flight control systems for undersea gliders focused, appropriately, on designing efficient steady motions and controlling the vehicles about these nominal motions [4]. More recent studies [6] have re-examined undersea glider design and control with a view toward even greater efficiency in nominal flight.

The transition from descent to ascent is a minor portion of an undersea glider's flight profile and has received little attention in flight control design. In this maneuver, the vehicle transitions from a stable, steady descending motion to a stable, steady ascending motion while maintaining forward flight. The locomotive force (i.e., the net weight) changes sign and the vehicle rotates by moving its center of mass. Graver [5] proposed a nine-state switched linear state feedback controller to negotiate the transition and illustrated the results in a simulation of *Slocum*. As Graver pointed out, however, existing undersea glider control systems are not so sophisticated. Typically, the net weight and center of mass are servo-controlled to pre-set positions that correspond to desired steady motions. "Flight control" consists of outer loop corrections to attain the desired pitch and heading angles [5]. While this approach works well for a vehicle in steady motion, operators have observed problems with stall when vehicles transition from descent to ascent. When this happens, the vehicle can lose directional stability, a situation which must be corrected with additional control effort when the vehicle finally approaches the desired steady, ascending flight condition [3].

This report uses an optimal control formulation to investigate control scheduling for an undersea glider in a symmetric pull-up. The motivation is to generate and characterize feasible state/control histories which involve a transition from steady, descending flight to steady, ascending flight. A primary objective is to prevent stall during this maneuver. The results may suggest a more informed open-loop control scheduling strategy for existing undersea glider flight control systems.

The initial findings in this report were presented at the 18th International Symposium on Mathematical Theory of Networks & Systems [7].

Section 2 develops the general dynamic model for an undersea glider and reviews the conditions for steady, wings level flight. Section 3 describes a simplified longitudinal dynamic model that is amenable to numerical optimization. Section 4 describes the optimal control formulation and presents the results of our numerical investigation. Conclusions and a brief

discussion of related, ongoing research efforts are provided in Section 6.

2 Vehicle Dynamic Model

The glider is modelled as a rigid body of mass m_{rb}. The vehicle displaces a volume of fluid of mass m_{f}. Define a net mass as $\bar{m} = m_{\mathrm{rb}} - m_{\mathrm{f}}$. If $\bar{m} = 0$, then the vehicle is neutrally buoyant. If $\bar{m} > 0$, the vehicle is heavy in water and tends to sink while if $\bar{m} < 0$, the vehicle is buoyant in water and tends to rise. For undersea gliders, $\bar{m}$ is typically modulated by an inflatable bladder, which changes the value of m_{f} by changing the displaced volume. Pitch and roll angles are controlled by moving an internal mass, shifting the center of gravity in relation to the center of buoyancy creating a moment that rotates the vehicle.

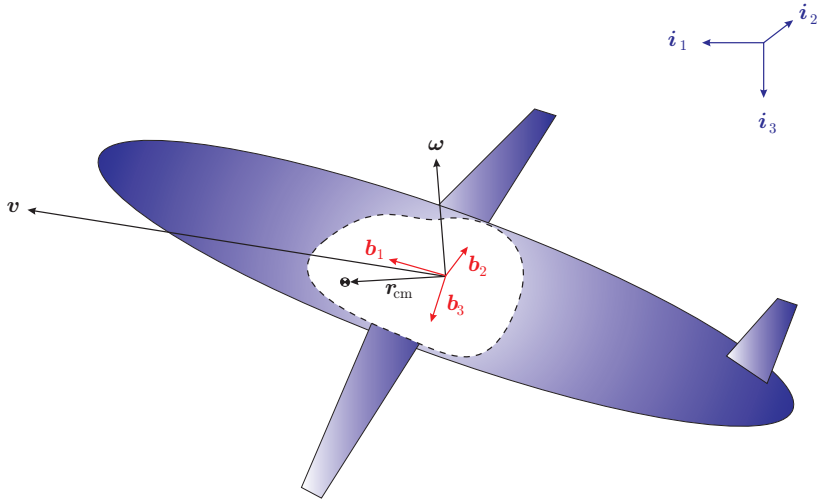

Figure 1: Reference frames.

Define a body-fixed, orthonormal reference frame represented by the unit vectors $\boldsymbol{b}_1$, $\boldsymbol{b}_2$, and $\boldsymbol{b}_3$, as in Figure 1. Define another orthonormal reference frame, denoted by the unit vectors $\boldsymbol{i}_1$, $\boldsymbol{i}_2$, and $\boldsymbol{i}_3$, which is fixed in inertial space such that $\boldsymbol{i}_3$ is aligned with the force due to gravity. The location of the body frame with respect to the inertial frame is given by the inertial vector $\boldsymbol{x} = [x,\ y,\ z]^T$. The orientation is given by the proper rotation matrix $\boldsymbol{R}_{\mathrm{IB}}$, which transforms free vectors from the body frame to the inertial frame.

2.1 Equations of Motion

Let $\boldsymbol{v} = [u,\ v,\ w]^T$ represent the translational velocity and let $\boldsymbol{\omega} = [p,\ q,\ r]^T$ represent the rotational velocity of the AUV with respect to inertial space, where $\boldsymbol{v}$ and $\boldsymbol{\omega}$ are both expressed in the body frame. The kinematic equations are

$$\dot{\boldsymbol{x}} = \boldsymbol{R}_{\mathrm{IB}}\boldsymbol{v} \tag{1}$$

$$\dot{\boldsymbol{R}}_{\mathrm{IB}} = \boldsymbol{R}_{\mathrm{IB}}\hat{\boldsymbol{\omega}} \tag{2}$$

where the character $\hat{\cdot}$ denotes the 3×3 skew-symmetric matrix satisfying $\hat{\boldsymbol{a}}\boldsymbol{b} = \boldsymbol{a} \times \boldsymbol{b}$ for vectors $\boldsymbol{a}$ and $\boldsymbol{b}$.

The rotation matrix $\boldsymbol{R}_{\mathrm{IB}}$ is typically parameterized using Euler angles. For aircraft and underwater vehicles, the most common choice of Euler angles are the roll angle ϕ, the pitch angle θ, and the yaw angle ψ. Let $\boldsymbol{e}_1$, $\boldsymbol{e}_2$, and $\boldsymbol{e}_3$ represent the standard orthonormal basis for $\mathbb{R}^3$. In terms of conventional Euler angles, the rotation matrix is

$$\boldsymbol{R}_{\mathrm{IB}}(\phi, \theta, \psi) = e^{\widehat{\boldsymbol{e}_3}\psi} e^{\widehat{\boldsymbol{e}_2}\theta} e^{\widehat{\boldsymbol{e}_1}\phi}.$$

Another reference frame which is commonly used in ocean vehicle dynamics is the "current frame," known as the "wind frame" in aircraft dynamics ($\underline{\boldsymbol{c}}_1$,$\underline{\boldsymbol{c}}_2$, $\underline{\boldsymbol{c}}_3$) . This frame is related to the body frame through the components of the body translational velocity vector. Define the two hydrodynamic angles

$$\alpha = \arctan\left(\frac{w}{u}\right) \qquad \text{and} \qquad \beta = \arcsin\left(\frac{v}{V}\right), \tag{3}$$

where $V = \|\boldsymbol{v}\|$. To transform a vector from the current frame to the body frame, one applies the proper rotation

$$\boldsymbol{R}_{\mathrm{BC}}(\alpha, \beta) = e^{-\widehat{\boldsymbol{e}_2}\alpha} e^{\widehat{\boldsymbol{e}_3}\beta}.$$

For example, one may transform the velocity vector from the current frame to the body frame as follows:

$$\boldsymbol{v} = \boldsymbol{R}_{\mathrm{BC}}(\alpha, \beta)(V\underline{\boldsymbol{c}}_1) = \begin{pmatrix} V\cos\alpha\cos\beta \\ V\sin\beta \\ V\sin\alpha\cos\beta \end{pmatrix}. \tag{4}$$

The linear momentum of the body/fluid system, expressed in the body frame, is denoted $\boldsymbol{p}$. The angular momentum is denoted $\boldsymbol{h}$. The vectors $\boldsymbol{p}$ and $\boldsymbol{h}$ are the conjugate momenta corresponding to $\boldsymbol{v}$ and $\boldsymbol{\omega}$, respectively. Thus,

$$\begin{pmatrix} \boldsymbol{p} \\ \boldsymbol{h} \end{pmatrix} = \begin{pmatrix} \boldsymbol{M} & \boldsymbol{C}^T \\ \boldsymbol{C} & \boldsymbol{I} \end{pmatrix} \begin{pmatrix} \boldsymbol{v} \\ \boldsymbol{\omega} \end{pmatrix} \tag{5}$$

where the 3×3 sub-matrices $\boldsymbol{M}$, $\boldsymbol{C}$, and $\boldsymbol{I}$ define the 6×6 *generalized inertia matrix*, which includes both the rigid body inertia and the *added* inertia due to the fluid. The dynamic equations are

$$\dot{\boldsymbol{p}} = \boldsymbol{p} \times \boldsymbol{\omega} + \bar{m}g\left(\boldsymbol{R}_{\mathrm{IB}}^T \boldsymbol{i}_3\right) + \boldsymbol{f}_{\mathrm{v}}(\boldsymbol{v}, \boldsymbol{\omega}) \tag{6}$$

$$\dot{\boldsymbol{h}} = \boldsymbol{h} \times \boldsymbol{\omega} + \boldsymbol{p} \times \boldsymbol{v} + m_{\mathrm{rb}} g \boldsymbol{r}_{\mathrm{cm}} \times \left(\boldsymbol{R}_{\mathrm{IB}}^T \boldsymbol{i}_3\right) + \boldsymbol{m}_{\mathrm{v}}(\boldsymbol{v}, \boldsymbol{\omega}) \tag{7}$$

where $\boldsymbol{f}_{\mathrm{v}}$ and $\boldsymbol{m}_{\mathrm{v}}$ represent the force and moment due to viscous flow effects and $\boldsymbol{r}_{\mathrm{cm}}$ is the location of the vehicle center of mass. Typically, one writes $\boldsymbol{f}_{\mathrm{v}}$ in terms of its three components in the current frame: drag force $\mathcal{D}$, side force $\mathcal{S}$, and lift force $\mathcal{L}$. The viscous moment is expressed in terms of its three components in the body frame: roll moment L, pitch moment M, and yaw moment N. Thus, we have

$$\boldsymbol{f}_{\mathrm{v}}(\boldsymbol{v}, \boldsymbol{\omega}) = -\boldsymbol{R}_{\mathrm{BC}}(\alpha, \beta) \begin{pmatrix} \mathcal{D}(\boldsymbol{v}, \boldsymbol{\omega}) \\ \mathcal{S}(\boldsymbol{v}, \boldsymbol{\omega}) \\ \mathcal{L}(\boldsymbol{v}, \boldsymbol{\omega}) \end{pmatrix} \qquad \text{and} \qquad \boldsymbol{m}_{\mathrm{v}}(\boldsymbol{v}, \boldsymbol{\omega}) = \begin{pmatrix} L(\boldsymbol{v}, \boldsymbol{\omega}) \\ M(\boldsymbol{v}, \boldsymbol{\omega}) \\ N(\boldsymbol{v}, \boldsymbol{\omega}) \end{pmatrix}.$$

Equations (1),(2), (6), and (7) describe the motion of a *rigid* undersea glider in inertial space. Given that our immediate aim is simply to characterize steady, wings level gliding motions, we have omitted the dynamics of the moving mass actuator from this model. In fact, in Section 3, we specialize further to a point mass model of the undersea glider, a standard practice in flight trajectory optimization. For a higher-dimensional vehicle model, which includes the internal actuator dynamics, see [1] or [5].

In studying steady motions, we typically ignore the translational kinematics (1). Moreover, the structure of the dynamic equations (6) and (7) is such that only the "tilt vector"

$$\boldsymbol{\zeta} = \boldsymbol{R}_{\mathrm{IB}}^{T} \boldsymbol{i}_3$$

is required to express the dynamics, allowing us to replace the matrix equation (2) for the rotational kinematics with the equation for $\dot{\boldsymbol{\zeta}}$. We therefore consider the following, reduced set of equations:

$$\dot{\boldsymbol{\zeta}} = \boldsymbol{\zeta} \times \boldsymbol{\omega} \tag{8}$$

$$\dot{\boldsymbol{p}} = \boldsymbol{p} \times \boldsymbol{\omega} + \bar{m} g \boldsymbol{\zeta} + \boldsymbol{f}_{\mathrm{v}}. \tag{9}$$

$$\dot{\boldsymbol{h}} = \boldsymbol{h} \times \boldsymbol{\omega} + \boldsymbol{p} \times \boldsymbol{v} + m_{\mathrm{rb}} g \boldsymbol{r}_{\mathrm{cm}} \times \boldsymbol{\zeta} + \boldsymbol{m}_{\mathrm{v}} \tag{10}$$

2.2 Wings Level Gliding Flight

The conditions for wings level, gliding flight are that $\boldsymbol{\omega} = \boldsymbol{0}$, $\boldsymbol{v} \cdot \boldsymbol{e}_2 = 0$, and $\boldsymbol{\zeta} \cdot \boldsymbol{e}_2 = 0$. The second condition implies that $v = 0$ and therefore that $\beta = 0$. The third condition implies that $\phi = 0$. Assume a nominal velocity $\boldsymbol{v}_0 = [u_0,\ 0,\ w_0]^T$ or, equivalently, nominal values of speed V_0 and angle of attack α_0. Substituting all of these conditions into equations (8) through (10), one obtains a corresponding center of mass location $\boldsymbol{r}_{\mathrm{cm}}$, *flight path angle* $\gamma_0 = \theta_0 - \alpha_0$, and net weight $\bar{m}_0 g$; see [8] and references therein.

The equilibrium values of $\boldsymbol{r}_{\mathrm{cm}}$, γ_0, and $\bar{m}_0$ depend on the system parameters and on the lift and drag model as well as the speed and angle of attack. Let $\bar{q}(V)$ denote the dynamic pressure:

$$\bar{q}(V) = \frac{1}{2} \rho V^2$$

where ρ is the fluid density, which is assumed to remain constant. Let S represent a reference area such as the wing planform area. Dimensional analysis shows that, in steady, symmetric flight, the drag and lift force may be written in terms of dimensionless coefficients as follows:

$$\mathcal{D}(V, \alpha) = C_D(\alpha) \bar{q}(V) S \qquad \text{and} \qquad \mathcal{L}(V, \alpha) = C_L(\alpha) \bar{q}(V) S$$

where

$$C_D(\alpha) = C_{D_0} + K \left(C_L(\alpha) \right)^2 \qquad \text{and} \qquad C_L(\alpha) = C_{L_\alpha} \alpha.$$

Figure 2 shows the wings level equilibrium glide characteristics for the dynamic model given in [1] for the *Slocum* electric glider with the wing surface area as the reference area: $S = 0.1327$ m^2. The lift and drag parameters are:

$$C_{L_\alpha} = 2.04 \text{ rad}^{-1}, \qquad C_{D_0} = 0.03, \qquad \text{and} \qquad K = 0.16.$$

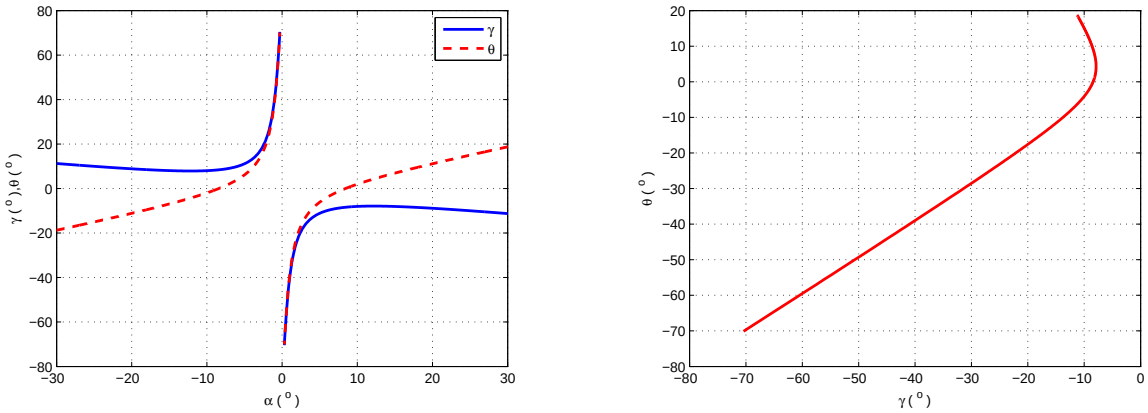

(a) $\theta(\alpha)$ and $\gamma(\alpha)$. (b) θ versus γ.

Figure 2: Equilibrium glide characteristics for the *Slocum* model in [1].

Figure 2(a) illustrates a fundamental obstacle in transitioning an undersea glider from descending to ascending flight at constant speed: the equilibrium manifold is discontinuous when α is zero. There can be no "quasi-steady" transition from downward to upward flight at constant speed.

3 Longitudinal Dynamics: Point Mass Model

In this note, we consider only symmetric motions, i.e., motions confined to the vehicle's plane of symmetry. Recalling that $\beta \equiv 0$ for longitudinally symmetric motions, we have from (4)

$$\begin{pmatrix} \dot{V} \\ V\dot{\alpha} \end{pmatrix} = \begin{pmatrix} \cos\alpha & \sin\alpha \\ -\sin\alpha & \cos\alpha \end{pmatrix} \begin{pmatrix} \dot{u} \\ \dot{w} \end{pmatrix}. \tag{11}$$

Ignoring inviscid hydrodynamic coupling between pitch and heave motions, we find from the first and third components of equation (9) that

$$\begin{pmatrix} m_u\dot{u} \\ m_w\dot{w} \end{pmatrix} = \begin{pmatrix} -m_w wq \\ m_u uq \end{pmatrix} + \bar{W}\begin{pmatrix} -\sin\theta \\ \cos\theta \end{pmatrix} - \begin{pmatrix} \cos\alpha & -\sin\alpha \\ \sin\alpha & \cos\alpha \end{pmatrix} \begin{pmatrix} \mathcal{D} \\ \mathcal{L} \end{pmatrix} \tag{12}$$

where $\bar{W} = \bar{m}g$.

At this point, we make a key assumption to simplify the optimal control problem developed in Section 4. We assume that $m_u = m_w$ and, for notational simplicity, we define $m = m_u = m_w$.

While added mass is not generally the same in surge and heave for an undersea vehicle, the assumption considerably simplifies the optimal control problem formulation. Our aim is an improved understanding of control scheduling for an undersea glider in a pull-up and we expect analysis results for this simplified model to provide valuable insight. Substituting (12) into (11), with $m_u = m_w = m$, the translational dynamic equations simplify to

$$\begin{pmatrix} \dot{V} \\ V\dot{\alpha} \end{pmatrix} = \begin{pmatrix} 0 \\ Vq \end{pmatrix} + \frac{1}{m}\bar{W}\begin{pmatrix} -\sin\gamma \\ \cos\gamma \end{pmatrix} - \frac{1}{m}\begin{pmatrix} \mathcal{D}(V,\alpha) \\ \mathcal{L}(V,\alpha) \end{pmatrix}$$

where $\gamma = \theta - \alpha$. For notational simplicity, we normalize the three forces by mass:

$$\tilde{W} = \frac{1}{m}\bar{W}, \qquad \tilde{D}(V,\alpha) = \frac{1}{m}\mathcal{D}(V,\alpha), \qquad \text{and} \qquad \tilde{L}(V,\alpha) = \frac{1}{m}\mathcal{L}(V,\alpha).$$

Taking α and $U = \frac{d\tilde{W}}{dt}$ as inputs, we have the following two-input dynamic model:

$$\begin{pmatrix} \dot{V} \\ \dot{\gamma} \\ \dot{\tilde{W}} \end{pmatrix} = \begin{pmatrix} -\tilde{W}\sin\gamma - \tilde{D}(V,\alpha) \\ \frac{1}{V}\left(-\bar{W}\cos\gamma + \tilde{L}(V,\alpha)\right) \\ U \end{pmatrix}. \tag{13}$$

4 Optimal Control Problem

We consider the model (13) of vertical plane motions for an undersea glider and study the control of transition from dive to climb. It has been observed that such transitions can exhibit large angle of attack (AoA) values resulting in degraded heading stability [3]. It is of interest to find transition strategies that limit these AoA excursions.

In practice, the inputs (α and U) are subject to upper and lower bounds. In lieu of bounds on the control, our cost functional will employ the usual quadratic integral (control effort) as follows:

$$J = \frac{1}{2}\int_0^{t_f} \left(R_\alpha \left(\frac{\alpha(t)}{\alpha_{\text{ref}}}\right)^2 + R_U \left(\frac{U(t)}{U_{\text{ref}}}\right)^2 \right) \mathrm{d}t \tag{14}$$

where R_α and R_U are control penalty weights and α_{ref} and U_{ref} are reference values. We take $\alpha_{\text{ref}} = 1$ radian and $U_{\text{ref}} = 1$ (m/s^2)/s. Initial conditions at time $t_0 = 0$ and final conditions at a specified final time $t = t_f$ are given for all three states:

$$V(t_0) = V_0, \qquad \gamma(t_0) = \gamma_0, \qquad \tilde{W}(t_0) = \tilde{W}_0 \tag{15}$$

$$V(t_f) = V_f, \qquad \gamma(t_f) = \gamma_f, \qquad \tilde{W}(t_f) = \tilde{W}_f \tag{16}$$

Our (open-loop) optimal control problem is to determine control histories $\alpha(\cdot)$, $U(\cdot)$ to transfer the dynamic model (13) from initial conditions (15) to end conditions (16) while minimizing the cost functional (14).

To study this problem we used *Pontryagin's Minimum Principle* [9] to derive a two-point boundary value problem (TPBVP) that characterizes extremal state/control trajectories. Numerical solutions of the TPBVP are candidates for optimality; they satisfy necessary conditions for optimality. Our motivation here is to produce feasible state/control paths that meet the end conditions.

4.1 Necessary Conditions

We begin with the usual variational Hamiltonian

$$\mathcal{H}(\lambda_V, \lambda_\gamma, \lambda_W, V, \gamma, \tilde{W}, \alpha, U) \triangleq -\lambda_V \left[\tilde{D}(V,\alpha) + \tilde{W}\sin\gamma\right] + \frac{\lambda_\gamma}{V}\left[\tilde{L}(V,\alpha) - \tilde{W}\cos\gamma\right] + \lambda_W U + \frac{\lambda_0}{2}\left(R_\alpha\left(\frac{\alpha(t)}{\alpha_{\text{ref}}}\right)^2 + R_U\left(\frac{U(t)}{U_{\text{ref}}}\right)^2\right)$$

The adjoint vector $(\lambda_V,\ \lambda_\gamma,\ \lambda_W)$ must satisfy the differential equations:

$$\dot{\lambda_V} = \lambda_V\frac{\partial\tilde{D}}{\partial V} - \frac{\lambda_\gamma}{V}\frac{\partial\tilde{L}}{\partial V} + \frac{\lambda_\gamma}{V^2}\left[\tilde{L}(V,\alpha) - \tilde{W}\cos\gamma\right] \tag{17}$$

$$\dot{\lambda_\gamma} = \lambda_V\tilde{W}\cos\gamma - \frac{\lambda_\gamma}{V}\tilde{W}\sin\gamma \tag{18}$$

$$\dot{\lambda_W} = \lambda_V\sin\gamma + \frac{\lambda_\gamma}{V}\cos\gamma\ , \tag{19}$$

whereas the $\mathcal{H}_{\min}$ optimality condition requires:

$$0 = -\lambda_V\frac{\partial\tilde{D}}{\partial\alpha} + \frac{\lambda_\gamma}{V}\frac{\partial\tilde{L}}{\partial\alpha} + \lambda_0\frac{R_\alpha}{\alpha_{\text{ref}}^2}\alpha \tag{20}$$

$$0 = \lambda_W + \lambda_0\frac{R_U}{U_{\text{ref}}^2}U\ . \tag{21}$$

As noted above, the drag coefficient is quadratic in α, so these equations are linear in the controls. For a *minimizer* we must have $\lambda_0\frac{R_\alpha}{\alpha_{\text{ref}}^2} - \frac{2KC_{L_\alpha}^2}{m}\bar{q}(V(t))\lambda_V(t) \geq 0$. We assume the problem is *normal* so that $\lambda_0 > 0$ and test this minimality condition along candidate extremals.

4.2 Two-Point Boundary Value Problem

Using extremal controls from (20, 21) we have a system of six differential equations (13 and 17-19) and six boundary conditions (15 and 16). We formulate a Newton problem with the initial values of the adjoints as (three) unknowns and the end-conditions (16) to be satisfied. This problem was solved numerically using the `fsolve` procedure in MATLAB (version R2007b). The underlying initial-value problem for the state/adjoint ODE system was solved using `ode45`.

4.3 Numerical Results

The problem of Section 4.2 was solved for a range of control weight ratios and final times. The lift and drag parameters, corresponding to the values used in [1] for the *Slocum* vehicle, are given near the end of Section 2.2. Other relevant parameters are:

$$m = 50\text{ kg}, \qquad S = 0.1327\text{ m}^2, \qquad \text{and} \qquad \rho = 1027\text{ kg/m}^3.$$

The six boundary conditions (15 and 16) were the same for each case:

$$V_0 = 0.77 \text{ m/s}, \quad \gamma_0 = -12.7°, \quad \tilde{W}_0 = 0.124 \text{ m/s}^2$$
$$V_f = V_0, \quad \gamma_f = -\gamma_0, \quad \tilde{W}_f = -\tilde{W}_0$$

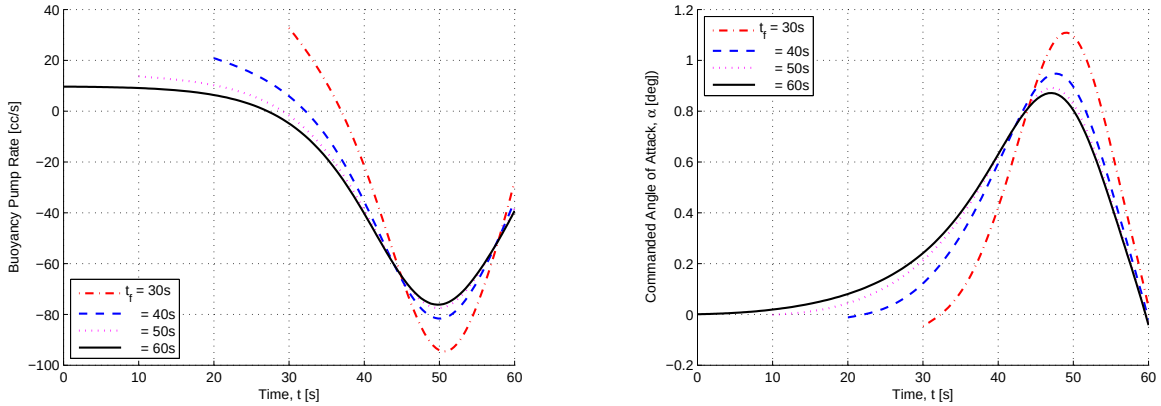

(a) Pump rate history: $U(t)$.

(b) AoA history: $\alpha(t)$.

Figure 3: Control histories for four values of t_f ($R_U = R_\alpha = 100$).

Figures 3 and 4 show state and control histories for four final times ($t_f \in \{30\text{ s}, 40\text{ s}, 50\text{ s}, 60\text{ s}\}$) with control penalty weights $R_\alpha = R_U = 100$ (a $1:1$ ratio). (The initial times are shifted in the figures to allow comparison of the final values.) Although four choices of t_f are shown, the qualitative behavior is similar in each case. Figure 3(a) shows that, in every case, the pump rate is initially *positive*, indicating that the vehicle is further *decreasing* its buoyancy. The AoA history, shown in Figure 3(b), begins near zero. For the vehicle described in [1], the initial conditions correspond to an equilibrium angle of attack around 4.3°, so this near-zero initial value of α suggests an initial nose-down maneuver. The combination of increased weight and decreased drag from the lower AoA leads to increased speed as shown in Figure 4(a).

Note that longer durations t_f correspond to larger, negative flight path angles and larger peak velocities. At some intermediate time, as seen in Figure 3(a), the pump rate becomes negative. Correspondingly, in the last ten seconds of the maneuver, as indicated in Figure 4(c), the net weight crosses through zero indicating that the vehicle has become positively buoyant. Figure 3 confirms one's intuition that a shorter execution time requires larger peak values of the control inputs (notably the buoyancy pump rate). The pump rate magnitudes are large for deep-sea gliders, but are of the same order as pump rates seen in existing shallow-water gliders. Note that the angle of attack remains well below the stall value; smaller values of α correspond to lower drag and increased kinetic energy to help carry the vehicle through the maneuver.

Figures 5 and 6 show state and control histories with $t_f = 30$ seconds, $R_U = 100$, and three different values of $R_\alpha \in \{1, 10, 100\}$, corresponding to ratios of $100:1$, $10:1$, and $1:1$. Also shown is the case where the pump rate is *fixed* at the constant value that satisfies

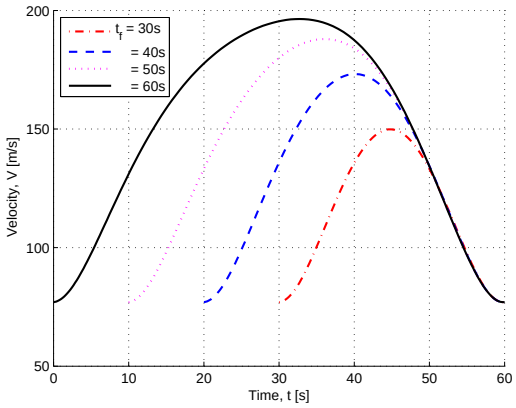

(a) Velocity history: $V(t)$.

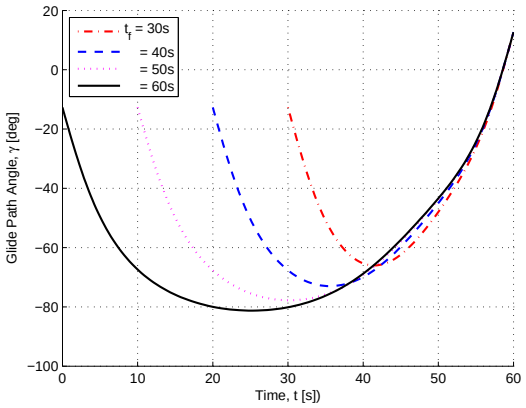

(b) Flight path angle history: $\gamma(t)$.

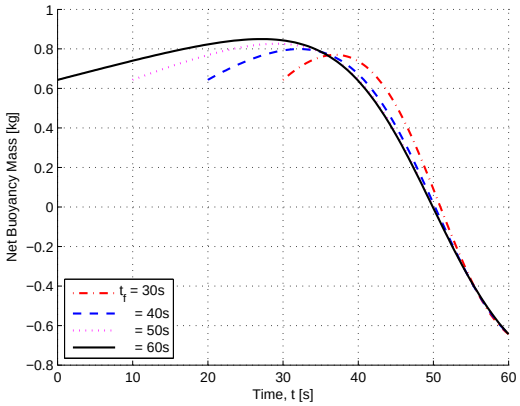

(c) Net weight history: $\tilde{W}(t)$.

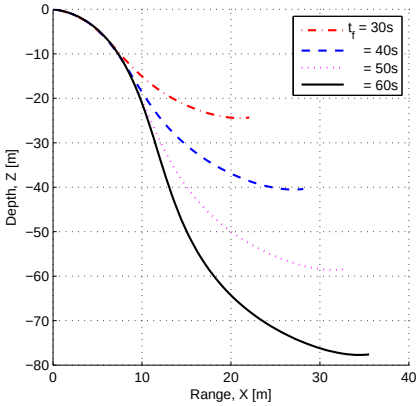

(d) Flight path.

Figure 4: State histories for four values of t_f ($R_U = R_\alpha = 100$).

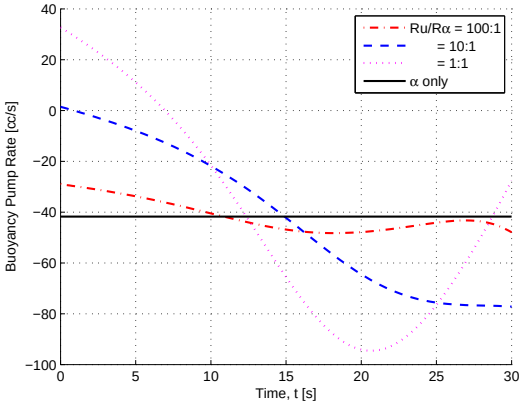

(a) Pump rate history: $U(t)$.

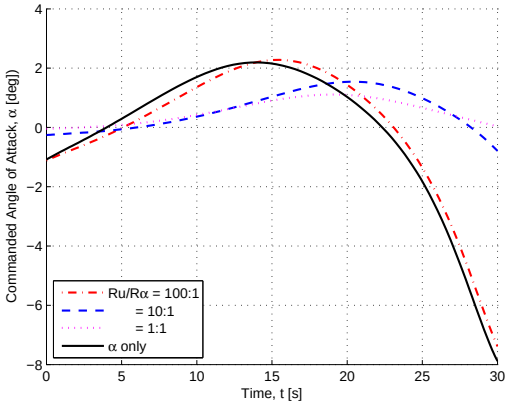

(b) AoA history: $\alpha(t)$.

Figure 5: Control histories with $t_f = 30$ seconds for three choices of R_U/R_α.

$\tilde{W}_f = -\tilde{W}_0$. In practical scenarios, the pump dynamics may be considerably slower than the servomotor dynamics, suggesting increased reliance on the center of mass (or AoA, in our simplified model) for longitudinal motion control. Figure 5 illustrates that a relatively large ratio R_U/R_α should lead to smaller pump rates and correspondingly larger AoA excursions. The figure suggests that the constant value of the pump rate approximates the extremal pump rate history as the penalty ratio R_U/R_α increases.

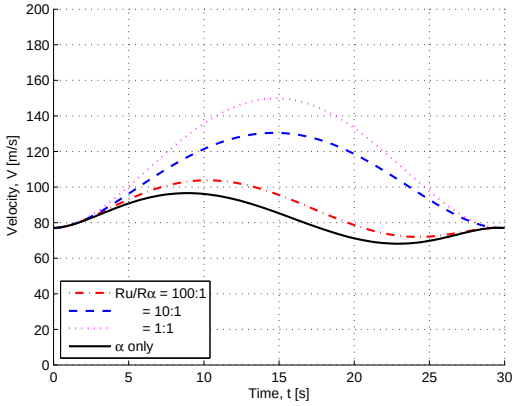

(a) Velocity history: $V(t)$.

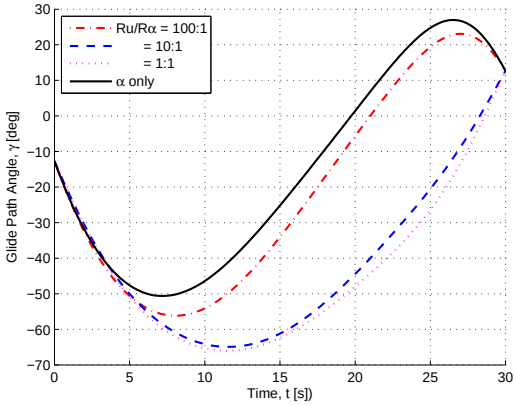

(b) Flight path angle history: $\gamma(t)$.

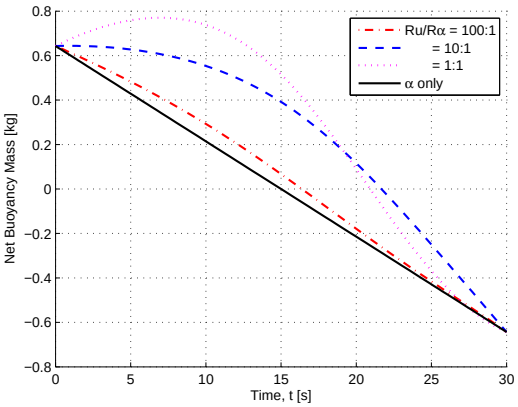

(c) Net weight history: $\tilde{W}(t)$.

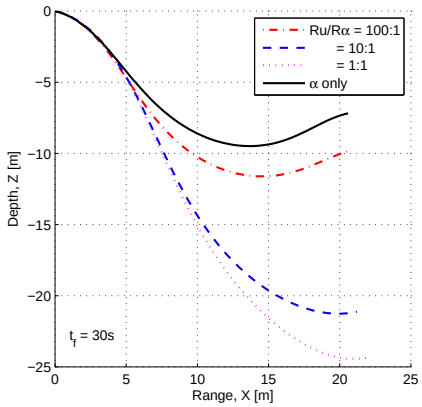

(d) Flight path.

Figure 6: State histories with $t_f = 30$ seconds for three choices of R_U/R_α.

As one would expect, larger penalties on the pump rate lead to lower peak velocities (Figure 6(a)) and shallower flight paths (Figure 6(b)) as the vehicle "bottoms out," however the qualitative behavior in all four cases is similar. An interesting feature of the flight path angle history in Figure 6(b) is the "pushover" that occurs in the final few seconds for the cases of a large pump rate penalty ($R_U/R_\alpha = 100$) and a constant pump-rate. This pushover phenomenon corresponds, in time, to a deceleration below the nominal speed as seen in Figure 6(a). In these cases, it appears that the vehicle develops insufficient kinetic energy to carry it through the pull-up, as indicated by the relatively large negative AoA near the end of the maneuver; see Figure 5(b).

4.4 Alternative Solution Methods

In addition to using Pontryagin's Minimum Principle to set up and solve a TPBVP, two more numerical methods were used for comparison. First, a POST[1]-like code was used. The second method used DIDO [10]–a commercially available add-in for Matlab that uses pseudospectral approximation theory [11] to numerically calculate a solution.

POST-like Solution Method. Our POST implementation imposes a user-specified grid on the time-axis, including nodes at the beginning and the end times. Within each panel the value of the control is constant; the collection of control values are unknowns in a Nonlinear Programming (NLP) formulation. The states are propagated over each panel by solving an initial-value problem (Matlab's `ode45`), while `fmincon` from the Optimization Toolbox is used to (iteratively) solve the NLP problem. Jacobians are not required but can be supplied by the user. In this application they were included and improved convergence.

DIDO Solution Method. Similar to the POST-like method, DIDO uses a numerical approximation based at nodes, but spaces them according to a Legendre-Gauss-Lobato scheme. The NLP unknowns in the DIDO formulation include both controls and states. The dynamics are approximated by a collocation procedure; the resulting algebraic equations are equality constraints in the NLP problem which is solved via the SNOPT software `http://www.sbsi-sol-optimize.com/asp/sol_product_snopt.htm`. The Jacobians are computed by finite-differencing; they cannot be supplied by the user.

DIDO was the easiest of the three methods to set up and initially run. All three solution methods arrived at the same trajectories–an initial pitch down, acceleration, then transitioning to the final equilibrium climbing state (see Figure 7). There were one or two overshoots of the final speed as the vehicle stabilized.

[1]Program to Optimize Simulate Trajectories [2]

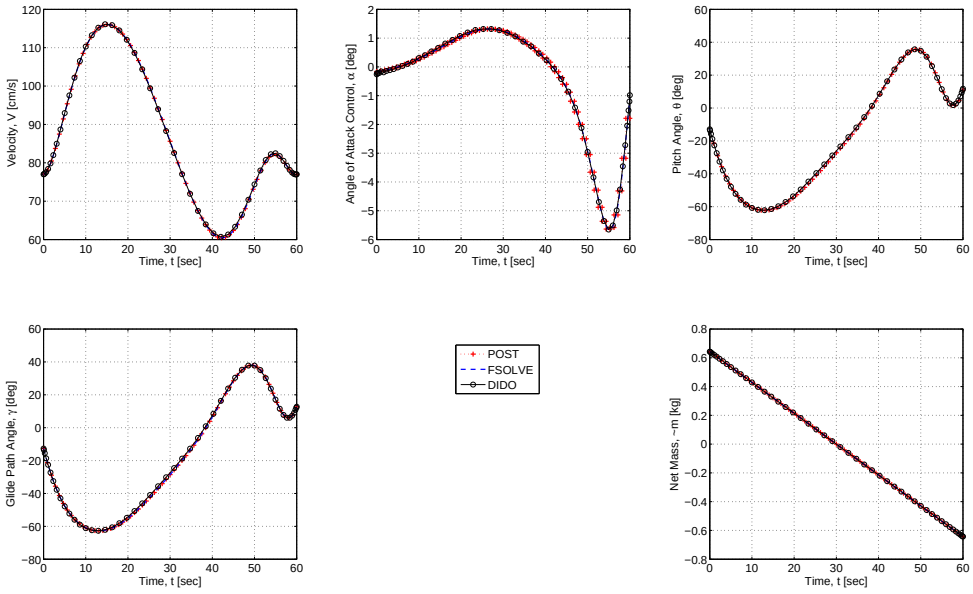

Figure 7: Three-state solution method comparison.

5 Longitudinal Dynamics: Rigid Body Model

The model was changed to include three more state variables and to make the rate of change of the longitudinal center of mass position the control, rather than AoA. The rate of change of the net mass (buoyancy pump rate) was constant. The new equations of motion are:

$$
\begin{aligned}
\dot{V} &= Vq\sin\alpha\cos\alpha\left(\frac{m_u}{m_w}-\frac{m_w}{m_u}\right)-\frac{\tilde{W}}{m_u}\cos\alpha\sin\theta+\frac{\tilde{W}}{m_w}\sin\alpha\cos\theta \\
&\quad -\mathcal{D}\left(\frac{\cos^2\alpha}{m_u}+\frac{\sin^2\alpha}{m_w}\right)+\mathcal{L}\cos\alpha\sin\alpha\left(\frac{1}{m_u}-\frac{1}{m_w}\right) \\
\dot{\alpha} &= q\left(\frac{m_w}{m_u}\sin^2\alpha+\frac{m_u}{m_w}\cos^2\alpha\right)+\frac{\tilde{W}}{V}\left(\frac{\sin\alpha\sin\theta}{m_u}+\frac{\cos\alpha\cos\theta}{m_w}\right) \\
&\quad +\frac{\mathcal{D}}{V}\cos\alpha\sin\alpha\left(\frac{1}{m_u}-\frac{1}{m_w}\right)-\frac{\mathcal{L}}{V}\left(\frac{\sin^2\alpha}{m_u}+\frac{\cos^2\alpha}{m_w}\right) \\
\dot{\theta} &= q \\
\dot{q} &= \frac{1}{I_{yy}}\left(\left(m_w-m_u\right)V^2\sin\alpha\cos\alpha+\mathcal{M}_\alpha\alpha+\mathcal{M}_q q-m_V g(X_{\mathrm{cm}}\cos\theta+Z_{\mathrm{cm}}\sin\theta)\right) \\
\dot{\tilde{W}} &= -2\tilde{W}_0/t_f \\
\dot{X}_{\mathrm{cm}} &= U_{X_{\mathrm{cm}}}
\end{aligned}
$$

Table 1: Initial and final equilibrium states.

Initial Conditions	Final Conditions
$V_0 = 77$ cm/s	$V_1 = 77$ cm/s
$\alpha_0 = 4.3°$	$\alpha_1 = -4.3°$
$\theta_0 = -8.4°$	$\theta_1 = 8.4°$
$q_0 = 0$ deg/s	$q_1 = 0$ deg/s
$\tilde{W}_0 = 6.18$ N	$\tilde{W}_1 = -6.18$ N
$X_{\mathrm{cm},0} = 1.3$ cm	$X_{\mathrm{cm},1} = -1.3$ cm

This model includes the added mass terms in the translation and pitch dynamics. It still assumes the process of moving the center of mass is small and slow enough to not affect the overall momenta.

Parameters The $\mathcal{L}$ift and $\mathcal{D}$rag profiles are as defined earlier. The pitch $\mathcal{M}$oment profile is described by two terms:

$$\mathcal{M}_\alpha = C_{\mathcal{M}_\alpha}\bar{q}S\bar{c} \qquad \mathcal{M}_q = C_{\mathcal{M}_q}\bar{q}S\bar{c}$$
$$C_{\mathcal{M}_\alpha} = -0.15 \qquad C_{\mathcal{M}_q} = -10.0$$

where

$$\begin{aligned} \bar{c} &= 0.1311 \text{ m} \\ I_{yy} &= 13.177 \text{ kg} \cdot \text{m}^2 \end{aligned}$$

The vertical position of the center of mass was fixed at $Z_{\mathrm{cm}} = 5$ cm below the centerline. The combined initial and final (equilibrium) conditions were prescribed as shown in Table 1.

This model was solved using DIDO over a time period of 60 seconds using 50 nodes. The results were compared against a simplified control history, in which there was a fixed buoyancy change rate over the entire interval and a fixed center of mass shift centered at the middle of the maneuver. This method was more realistic than shifting the center of mass at the beginning of the maneuver.

The simplified control scheme (Figures 8 and 9) caused the vehicle to slow down as net mass decreased, then pitch up during the center of mass shift, increasing the angle of attack. The faster the center of mass was shifted, the larger the angle of attack excursion. If the total duration of the buoyancy change was extended to more than 60 seconds, the vehicle slowed more and the angle of attack increased. Two different optimized solutions are plotted for comparison: The original 3-state model with fixed buoyancy rate change and the updated 6-state model. The 6-state model has more overall movement of the center of mass than the simplified model, but controlled the speed better throughout the manuever. Also, the 6-state optimized solution was qualitatively similar to the 3-state model which used angle of attack as the control. However, the 6-state model had smaller speed and pitch angle excursions and more accurately modelled existing underwater glider operation.

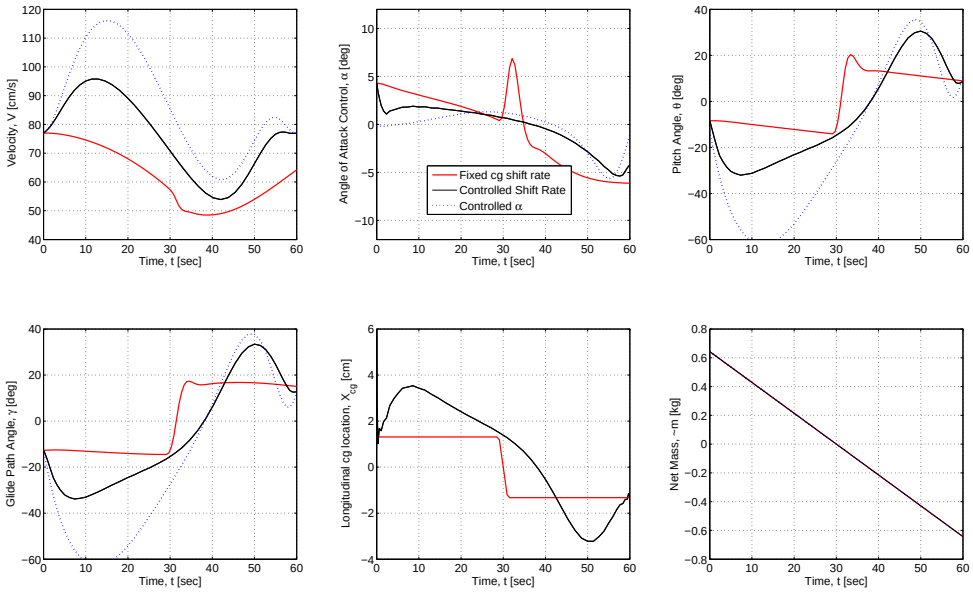

Figure 8: Fixed rate model comparison with optimized models.

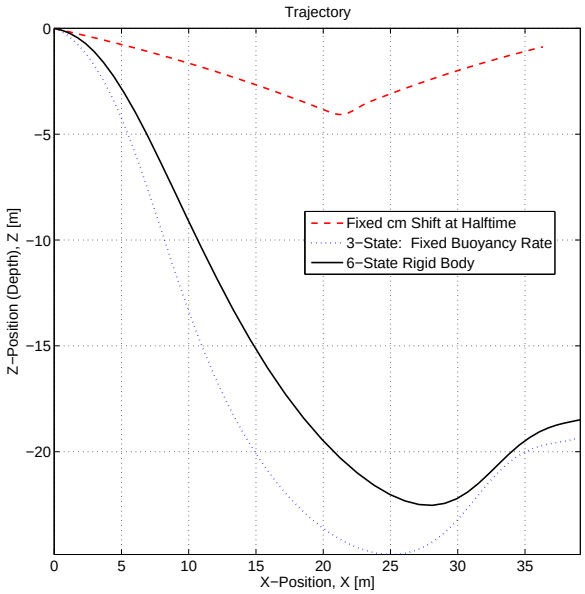

Figure 9: Trajectory Comparisons.

Figure 10 compares the effects of including added mass terms: $m_u = 52.3$ kg and $m_w = 116.6$ kg. The trajectories are almost identical. The relatively small angles of attack experienced in this maneuver (less than 10°), show that the vehicle is "flying" through the water nose forward and not pitched up with it's bottom side forward. This negated most of the effect

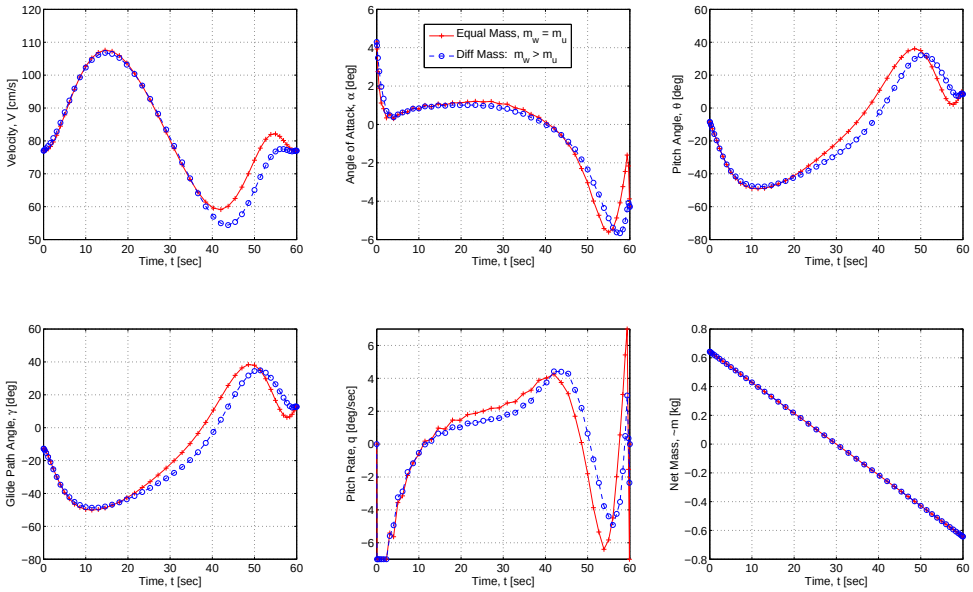

Figure 10: Solution including added mass effects.

of the larger m_w mass term.

6 Conclusions

An optimal control formulation was used to investigate control scheduling for an undersea glider in a symmetric pull-up. The objective was to generate and characterize feasible state/control histories which transition the vehicle from steady descending flight to steady ascending flight while avoiding stall. The results suggest that, if the buoyancy pump is capable of relatively large pump rates, an effective strategy is to initially increase the net weight and nose the vehicle down in order to gain kinetic energy to carry it through the pull-up while maintaining a small angle of attack. In cases where pump rate control was not heavily penalized, relative to pitch control, the vehicle's speed remained larger than its nominal value throughout the pull-up. Also, the vehicle continued to descend throughout the majority of the maneuver. If the buoyancy pump rate is limited, this strategy may be less effective. In cases where the pump rate control was heavily penalized, or was held constant, the vehicle slowed below its nominal speed and began to rise just after becoming positively buoyant. The motion resulted in a marked "pushover" maneuver in the final moments to meet the specified boundary condition. The results described here may have implications for the both operation of existing undersea gliders and actuator sizing for future glider designs.

Acknowledgements. The authors are grateful to Nina Mahmoudian for her input concerning glider steady motions. This work was sponsored, in part, by AFOSR under Grant #FA9550-07-1-0273 and by ONR under Grant #N00014-08-1-0012.

References

[1] P. Bhatta. *Nonlinear Stability and Control of Gliding Vehicles*. PhD thesis, Princeton University, 2006.

[2] G.L. Brauer, D.E. Cornick, and R. Stevenson. Capabilities and applications of the program to optimize simulated trajectories. Technical Report NASA CR-2770, Martin Marietta Corporation, 1977.

[3] C. C. Eriksen, T. J. Osse, R. D. Light, T. Wen, T. W. Lehman, P. L. Sabin, J. W. Ballard, and A. M. Chiodi. Seaglider: A long-range autonomous underwater vehicle for oceanographic research. *Journal of Oceanic Engineering*, 26(4):424–436, 2001. Special Issue on Autonomous Ocean-Sampling Networks.

[4] A. M. Galea. Optimal path planning and high level control of an autonomous gliding underwater vehicle. Master's thesis, Massachusetts Institute of Technology, 1999.

[5] J. G. Graver. *Underwater Gliders: Dynamics, Control, and Design*. PhD thesis, Princeton University, 2005.

[6] S. A. Jenkins, D. E. Humphreys, J. Sherman, J. Osse, C. Jones, N. Leonard, J. Graver, R. Bachmayer, T. Clem, P. Carroll, P. Davis, J. Berry, P. Worley, and J. Wasyl. Underwater glider system study. Technical Report 53, Scripps Institution of Oceanography, May 2003.

[7] R. Kraus, E. Cliff, C. Woolsey, and J. Luby. Optimal control of an undersea glider in a symmetric pull-up. In *Proceedings of the 18th International Symposium on Mthermatical Theory of Networks and Systems*, Blacksburg, Virginia, 2008.

[8] N. Mahmoudian, J. Geisbert, and C. A. Woolsey. Steady turns and optimal paths for underwater gliders. In *AIAA Guidance, Navigation, and Control Conference*, Hilton Head Island, SC, August 2007. AIAA-2007-6602.

[9] L. S. Pontryagin, V.G. Boltyanskii, R. V. Gamkrelidze, and E. F. Mishchenko. *The Mathematical Theory of Optimal Processes*. Wiley-Interscience, 1962.

[10] I. Michael Ross. *A Beginner's Guide to DIDO (Ver 7.3): A MATLAB Application package for Solving Optimal Control Problems*. Elissar, LLC, Monterey, CA, 2007.

[11] I.M. Ross and F. Fahroo. Legendre pseudospectral approximations of optimal control problems. In *Lecture Notes in Control and Information Sciences*, pages 327–342. Springer-Verlag, New York, NY, 2003.

[12] J. Sherman, R. E. Davis, W. B. Owens, and J. Valdes. The autonomous underwater glider "Spray". *Journal of Oceanic Engineering*, 26(4):437–446, 2001. Special Issue on Autonomous Ocean-Sampling Networks.

[13] D. C. Webb, P. J. Simonetti, and C. P. Jones. SLOCUM: An underwater glider propelled by environmental energy. *Journal of Oceanic Engineering*, 26(4):447–452, 2001. Special Issue on Autonomous Ocean-Sampling Networks.